Invited paper

L.M. DOESWIJK
G. RIJNDERS
D.H.A. BLANK✉

Pulsed laser deposition: metal versus oxide ablation

Mesa+ Research Institute, Faculty of Science and Technology, University of Twente,
PO Box 217, 7500 AE Enschede, The Netherlands

ABSTRACT We present experimental results of pulsed laser interaction with metal (Ni, Fe, Nb) and oxide (TiO_2, $SrTiO_3$, $BaTiO_3$) targets. The influence of the laser fluence and the number of laser pulses on the resulting target morphology are discussed. Although different responses for metal and oxide targets to repetitive laser irradiation could be expected due to the different band structures of metals and oxides, the optical response is quite similar for 248-nm laser irradiation. Therefore, the difference in response is largely caused by differences in thermal properties. Metal targets show periodic structures of the order of micrometers after consecutive pulses of laser radiation, while the $SrTiO_3$ and $BaTiO_3$ targets show a flat surface after ablation for relatively low fluences ($1.0\,J\,cm^{-2}$). The observed TiO_2 target ablation characteristics fall in between those of the ablated metals and perovskites, because ablation results in the presence of Ti-rich material, which shields the underlying stoichiometric target material from ablation. The final target morphology is dependent on fluence, number of pulses, and the movement of the target itself (rotating, scanning, or stationary). It can take between 15 and 75 pulses to reach a steady-state target morphology on a stationary target.

PACS 79.20.Ds; 52.38.Mf; 81.15.Fg

1 Introduction

To achieve a better understanding of the relation between film deposition and the resulting film properties, more insight is needed in all the different stages of the pulsed laser deposition (PLD) process. The PLD process starts with ablation of target material. The flexibility of the PLD setup offers the researcher a large freedom of choice in target material and ablation characteristics. The large dynamic ranges possible for ablation parameters result in different regimes of ablation and deposition. A couple of thousand laser pulses irradiate the target during the deposition of a thin film. If the target surface were left unchanged after each pulse, every consecutive pulse would result in the same laser–target interaction and could be described by the same characteristics. Laser pulses, however, rarely remove material in a smooth

✉ Fax: +31-53/489-4683, E-mail: d.h.a.blank@utwente.nl

layer-by-layer fashion. Instead, the laser-irradiated target surface becomes altered, both physically and chemically.

The target surface characteristics can influence the ablation rate, the film stoichiometry, and the film-surface roughness. Depending on the exact target morphology, a rough target surface can either decrease or increase the ablation rate. The former is a result of an increased surface area and, therefore, reduced fluence, while the latter is the result of better light coupling into the target. If induced target surface structures are aligned in the direction of the laser beam, the plasma is also shifted in the direction of the laser beam. Exfoliation of fragile microstructures formed at the target surface results in rough film surfaces, because the loose debris is carried toward the substrate by the plasma where they condense onto the growing thin film. For multi-element materials, it is important to realize stoichiometric ablation [1, 2]. A first indication of stoichiometric ablation, though not sufficient, is a smooth target morphology, which also offers the possibility of a longer, stable use of the target. These requirements result in a critical ablation threshold, for which a desirable target morphology is obtained.

We present here the experimental results of pulsed laser interaction with metal (Ni, Fe, Nb) and oxide (TiO_2, $SrTiO_3$, $BaTiO_3$) targets. The influence of the laser fluence and the number of laser pulses on the resulting target morphology and chemical composition are discussed.

2 Target–laser interaction for metal and oxide targets

Photonic energy is coupled into the target via electronic processes [3, 4]. Photons interact with the outermost (bound or free) valence electrons of atoms. Metals are characterized by their loosely bound outermost electrons, which are essentially free to travel around from atom to atom. For irradiation of metals with light of frequencies much lower than the plasma frequency, absorption is controlled by the free carriers in the material. Electromagnetic radiation with such large wavelengths is, however, strongly reflected, requiring large laser-beam intensities to compensate for the large reflection losses. As the wavelength of the incident radiation decreases, the absorption and the reflectivity decrease. For even smaller wavelengths, the exact dependence of the optical parameters on wavelength depends on the specific band structure of the individual materials.
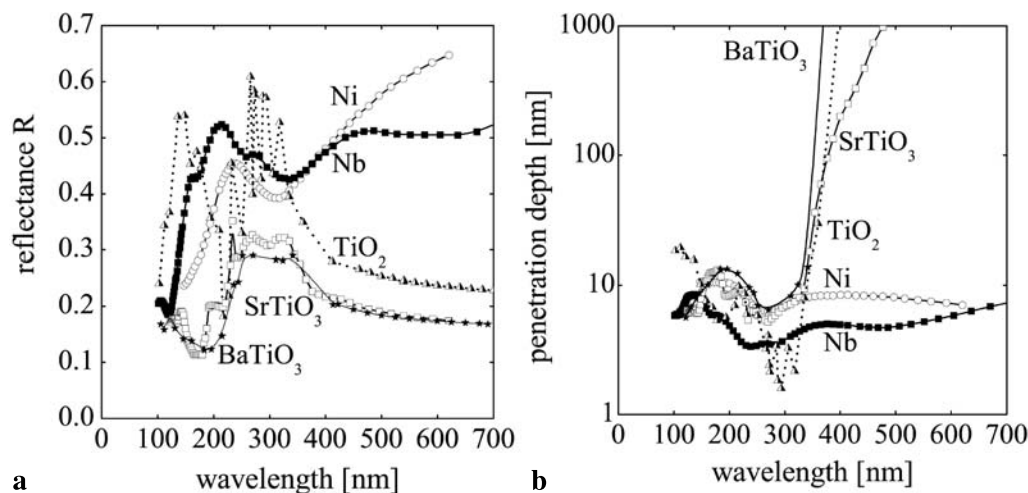
FIGURE 1 **a** Reflectance and **b** penetration depth as a function of wavelength of incident radiation for several target materials. The optical data (refractive index n and extinction coefficient k) were taken from [5, 6]

Unlike metals, the outermost electrons of insulators completely fill their shell. For radiation with a photon energy greater than the band gap E_g, electronic transitions between the valence and conduction bands are induced. Again, the strongly absorbing region of the spectrum coincides with the highest-reflectivity region. At energies below the band gap, the optical properties of insulators are determined by the much weaker intraband electronic transitions. Overall, insulators strongly resemble metals at wavelengths above their individual band edges, as indicated by the reflectance and penetration depth data given in Fig. 1. The optical data (refractive index n and extinction coefficient k) were taken from [5, 6]. Moreover, upon high-density irradiation ($> 10^8 \, \mathrm{W \, cm^{-2}}$), materials quickly pass into an absorbing state because of optical breakdown, reducing the difference between opaque and transparent materials [7, 8]. So, the optical properties of the metals and oxides presented in Fig. 1 are quite similar in the case of high energy density nanosecond laser irradiation of 248 nm. Therefore, the difference between metal and oxide target material removal is mainly determined by the thermal properties of the materials. An overview of some optical and thermal properties is given in Table 1 for the target materials used in this research.

The thermal diffusivity for the metals is on average $2.3 \times 10^{-5} \, \mathrm{m^2 \, s^{-1}}$ and for the oxides a factor of 10 lower ($3.2 \times 10^{-6} \, \mathrm{m^2 \, s^{-1}}$). If the optical absorption depth is much smaller than the thermal diffusion length, the laser energy is absorbed in the target-surface layer and the thermal diffusivity controls the heating characteristics. In the opposite case, the optical absorption depth mainly determines the ablation depth. The former is the case for the above-mentioned target materials for laser irradiation at 248 nm as shown in Table 1. Although the temperature dependence of the thermal and optical properties during laser ablation was disregarded, the use of constant thermal properties was sufficient to obtain a first indication of the difference between metal and oxide ablation.

3 Target morphology

3.1 *Experimental*

The laser ablation experiments were carried out with a KrF (248 nm) laser beam (Compex 205, Lambda Physik) with a pulse width of about 25 ns (FWHM). The beam entered the vacuum chamber at an angle of 45° with respect to the target normal. A mask was placed in the laser beam to reduce the spatial variation of the laser energy within the beam to less than 10%. The maximum pulse-to-pulse variation was 4%. The energy of the laser beam behind the mask was measured as an average over multiple pulses to calculate the laser fluence. Target morphology experiments were

Target material	Melting temperature	Reflectance	Penetration depth p	Thermal diffusion length l	Ratio p/l	Enthalpy of evaporation H_{ev}	Ablation threshold
	(1 atm) [K]	(248 nm)	(248 nm) [nm]	(300 K) [μm]	($\times 10^{-3}$)	($\times 10^5$) [J mol^{-1}]	(248 nm) [J cm^{-2}]
Ni	1728	0.45	6.7	1.1	6.1	4.5*	0.85$^+$–2.2
Fe	1811	0.43	7.8	1.1	7.1	3.5	2.0
Nb	2750	0.48	3.4	1.1	3.1	6.8	3.5
TiO$_2$	2095	0.34	5.8	0.4	14.5	17*	< 0.5
SrTiO$_3$	2353	0.23	6.3	0.4	15.8	30*	0.1
BaTiO$_3$	1898	0.13	7.8	0.3	26.0	30*	–

* Indication of a value for H_{ev} based on given enthalpies in [16] for lower temperatures
$^+$ Matthias et al. [15] reported a threshold of 0.85 J cm^{-2} for visible damage at the target surface by melting and an ablation threshold of 2.2 J cm^{-2} for plasma formation. Hiroshima et al. [14] reported a non-zero deposition rate at a fluence of 0.85 J cm^{-2}

TABLE 1 Overview of some optical and thermal properties for target materials used in this research [2, 5, 6, 9–19]

performed in vacuum on stationary targets of Ni (99.995%), Fe (99.995%), Nb (99.9%), and crystalline $SrTiO_3$, $BaTiO_3$, and TiO_2 (rutile). The target morphologies were investigated as a function of fluence (0.6–7.9 J cm^{-2}) and number of laser pulses (1–1000) by scanning electron microscopy (SEM). Target stoichiometry after ablation was investigated by X-ray photoelectron spectroscopy (XPS).

3.2 *Dependence on laser fluence*

For a specific laser and target, the fluence mainly determines the target morphology evolution under pulsed laser irradiation. Figure 2 shows the target morphology after 200 pulses on a stationary Nb target as a function of the incident laser fluence. The Nb target had an ablation threshold of 3.5 J cm^{-2}. The target morphology shows a periodic structure for fluences of 4.5 J cm^{-2} and higher. The 'waves' are perpendicular to the direction of the incoming laser beam. In the case of Fig. 2c, the laser beam came from the right-hand side, creating a steep, rougher side and a longer, smooth side of a wave. The target morphology after ablation of a stationary Fe target is shown in Fig. 3. The periodic structure for 7.0 J cm^{-2} shows a large similarity with the induced structure in the case of Nb ablation: a steep, rougher side and a longer, smooth side. For higher fluences, the waves become less straight. The period of the structure increased for increasing fluences (8.8 μm, 18.4 μm, and 21.2 μm in the case of Fe ablation for 100 pulses at 2.8 J cm^{-2}, 6.0 J cm^{-2}, and 7.9 J cm^{-2}, respectively). The target morphology in the case of Ni ablation is similar.

In the case of ablation of stationary $BaTiO_3$ and $SrTiO_3$ targets, the desirable smooth target morphology could be achieved. Figure 4 shows the target morphology after 200 pulses for a $SrTiO_3$ target as a function of laser fluence. A periodic structure is visible for a fluence of 0.6 J cm^{-2}, but for a fluence of 1.0 J cm^{-2} the periodicity disappears. The target morphology barely changed between 1.0 and 2.5 J cm^{-2}, and showed a flat surface with many cracks due to surface melting and subsequent fast solidification. The higher ablation threshold of metals in comparison with oxides is mainly caused by the higher reflectance and thermal diffusivity of metals. The former results in less photonic energy coupled into the target material and the latter results in a larger volume into which the absorbed energy diffuses.

Figure 5 shows the target morphology after 200 pulses on a stationary TiO_2 target as a function of laser fluence. The SEM images are quite different from the former results. The target morphology changes more strongly for the different fluences used. For a low fluence of 0.6 J cm^{-2}, no periodicity perpendicular to the direction of the incoming laser beam is clearly visible. A periodic structure is
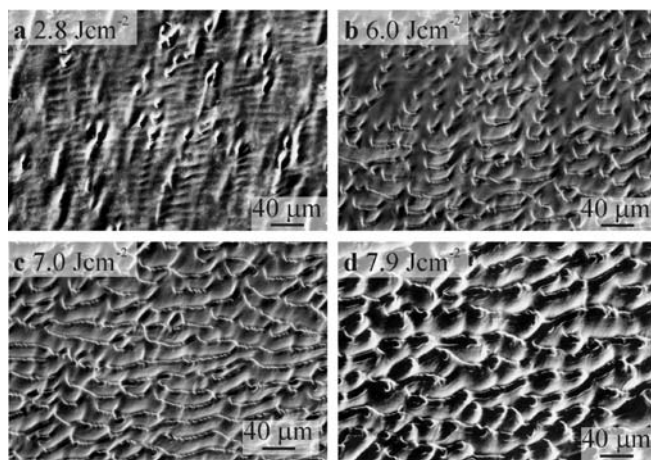

FIGURE 3 Fe target morphology after 100 pulses as a function of fluence for **a** 2.8 J cm^{-2}, **b** 6.0 J cm^{-2}, **c** 7.0 J cm^{-2}, and **d** 7.9 J cm^{-2}
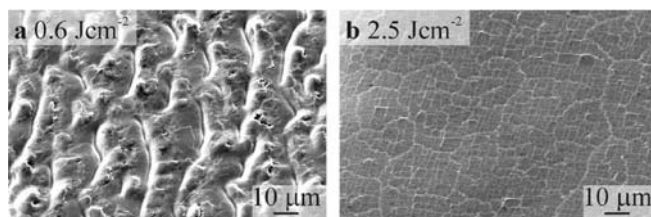
FIGURE 4 $SrTiO_3$ target morphology after 200 pulses at a fluence of **a** 0.6 J cm^{-2} and **b** 2.5 J cm^{-2}

present for ablation at 1.5 J cm^{-2}, though quite different from the case of metal or $SrTiO_3$ ablation. The target morphology shows a wavy pattern for higher fluences, even up to 6.0 J cm^{-2}. No flat target morphology was achieved for TiO_2 ablation. The waves are again perpendicular to the direction of the incoming laser beam, independent of the spot size and mask shape used. For the spot sizes used of 5 mm^2 of different shapes, the wave period is between 15 and 20 μm, which is the same order of magnitude as in the case of metal ablation. In the case of TiO_2, a fluence of at least 2.0 J cm^{-2} is recommended, since the target morphology contains loose debris for fluences under 2.0 J cm^{-2} as shown in Fig. 5c. The situation changes for a rotating target, because the ablation spots of consecutive pulses can partially overlap. Although overlap only occurred for a small range of angles of about ±10° (with 0° referring to complete overlap), the resulting target morphology changed drastically as shown in Fig. 5f in comparison with Fig. 5b. It appeared that the target morphology was already debris-free for a laser fluence of 1.5 J cm^{-2}, while for a laser fluence of 1.0 J cm^{-2} the target morphology still showed fragile microstructures. Atomic force microscopy images of TiO_2 films
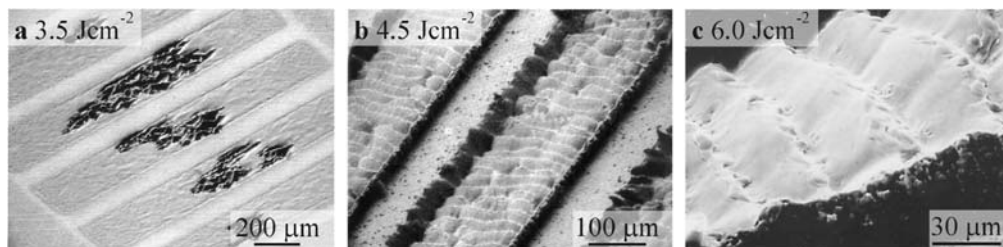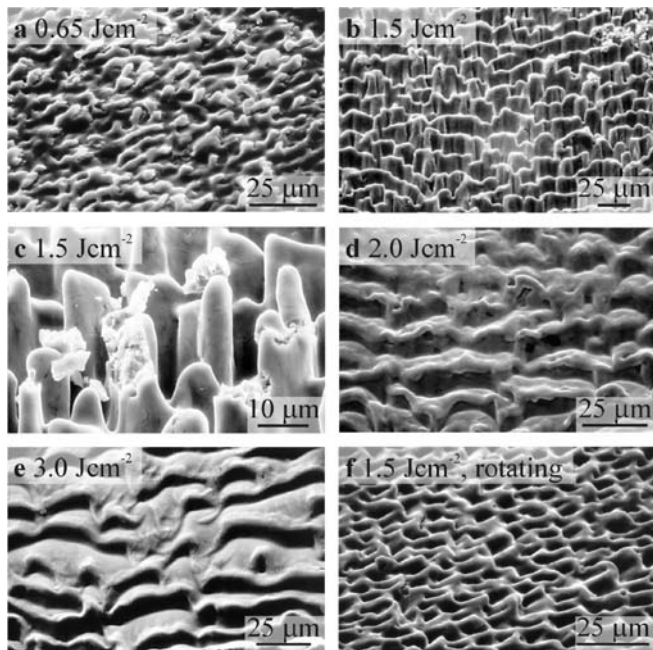

FIGURE 2 Nb target morphology after 200 pulses as a function of fluence for **a** 3.5 J cm^{-2}, **b** 4.5 J cm^{-2}, and **c** 6.0 J cm^{-2}. The mask used consisted of seven rectangular apertures of 7 × 2 mm^2
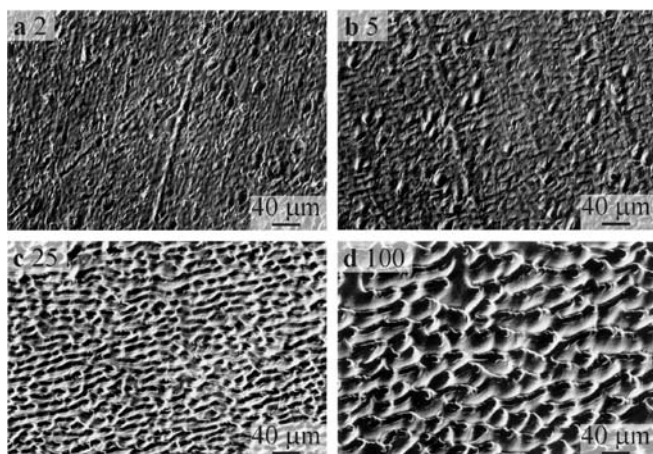
FIGURE 5   TiO$_2$ target morphology after 200 pulses as a function of fluence for **a** 0.65 J cm^{-2}, **b** 1.5 J cm^{-2}, **c** 1.5 J cm^{-2} enlarged, **d** 2.0 J cm^{-2}, **e** 3.0 J cm^{-2}, and **f** 1.5 J cm^{-2} on a rotating target

deposited at 1.0 J cm^{-2} showed that exfoliation, indeed, takes place.

3.3   *Dependence on number of pulses*

The resulting target morphologies also depend on the number of pulses used. Figure 6 shows this dependence in the case of Fe ablation at 7.9 J cm^{-2}. The SEM images of the target morphology after ablation as a function of number of pulses show similarity with the evolution of morphology as a function of fluence. After 25 pulses the basic surface structure does not change much, only the period of the structure increases for an increasing number of pulses as it does with increase of fluence.

The evolution of the target morphology of a TiO$_2$ target under consecutive irradiation with laser pulses of 2.0 J cm^{-2}

FIGURE 6   Fe target morphology after ablation at a fluence of 7.9 J cm^{-2} as a function of number of pulses. **a** 2, **b** 5, **c** 25, and **d** 100
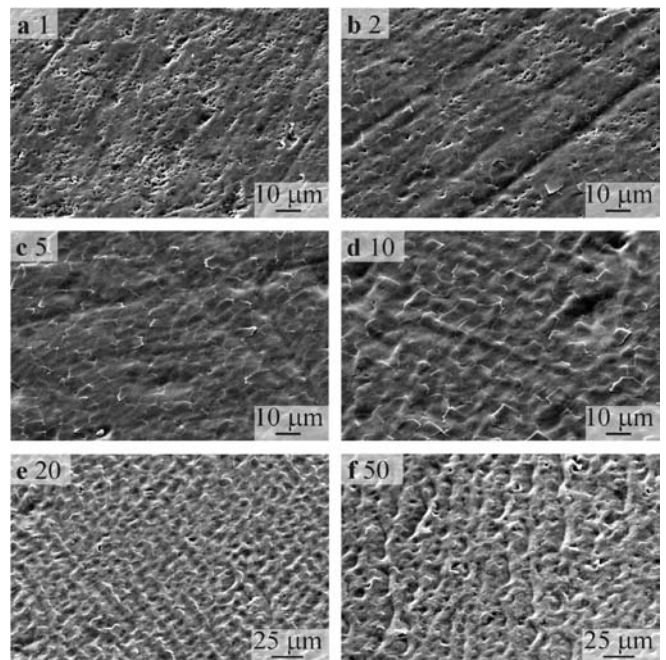

FIGURE 7   TiO$_2$ target morphology after ablation at a fluence of 2.0 J cm^{-2} as a function of number of pulses. **a** 0, **b** 1, **c** 2, **d** 5, **e** 10, **f** 20, **g** 50, **h** 75, and **i** 100

is presented in Fig. 7. The morphology after one laser pulse shows a lot of pits. Initial ablation of a SrTiO$_3$ target shows the same characteristic pits. Since these pits are not present in the case of metal ablation, the pits are assumed to be induced by the escape of oxygen gas. Consecutive pulses diminish the number of pits and induce the presence of cracks, indicative of solidification after melting. The first indication of the creation of periodic surface structures on the TiO$_2$ target is visible after 10 pulses and more clearly after 20 pulses. The steady-state regime is achieved between 50 and 75 pulses. In the case of SrTiO$_3$ ablation at 1.7 J cm^{-2}, the steady state is already reached after 15 pulses.

4   Oxygen reduction in oxide targets

In the case of the oxide targets, the repetitive laser irradiation not only changed the target morphology but also the target stoichiometry. As mentioned in Sect. 3.3, the pits present at the oxide target surface after irradiation with one laser pulse indicate the escape of oxygen gas from the target. In addition, the yellowish oxide target color changed into gray after ablation, indicative of a metal-rich layer. The electrical resistance of the TiO$_2$ target surface, determined by a two-probe measurement, decreased at least four orders of magnitude after ablation (the electrical resistance of the non-ablated oxide surface was higher than the maximum measurable resistance). The electrical resistance of the SrTiO$_3$ target surface decreased at least one order of magnitude. The stoichiometry of a TiO$_2$ target after ablation at 1.5 J cm^{-2} for 200 pulses was checked with XPS. Figure 8a shows the ratio of O and Ti atomic concentrations as a function of depth below the ablated target surface. The stoichiometry at the target surface is probably induced by the presence of CO and OH absorbates and by oxygen diffusion into the target during transport from
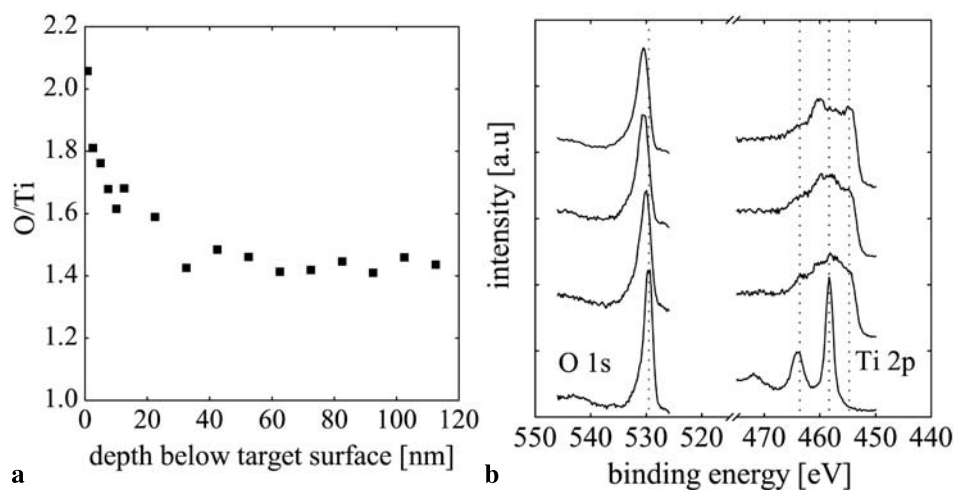
FIGURE 8 XPS measurements for an ablated TiO_2 target at 1.5 J cm^{-2} for 200 pulses. **a** Measured ratio of atomic concentrations of O and Ti as a function of depth below the ablated target surface, **b** a comparison of the measured O 1s and Ti 2p spectra at the surface of a fresh TiO_2 target (*lower line*), at 10 nm below the surface of a fresh TiO_2 target (*second line*), at 10 nm below the surface of an ablated TiO_2 target (*third line*), and at 122 nm below the surface of an ablated TiO_2 target (*upper line*)

the PLD system to the XPS setup. After about 60 nm from the target surface, the ratio O/Ti levels off to 1.43. Argon etching is known to induce preferential sputtering of oxygen from oxide samples. XPS measurements on a fresh TiO_2 target resulted in a final ratio of 1.8, which indicates the ablated target volume to be $TiO_{1.59}$. Thus, the repetitive laser irradiation resulted in an above-stoichiometric oxygen loss, leaving a metal-rich layer behind. This was confirmed by the obtained spectra, presented in Fig. 8b. The Ti 2p and O 1s spectra are presented as measured at the surface of a fresh TiO_2 target (lower line), at 10 nm below the surface of a fresh TiO_2 target (second line), at 10 nm below the surface of an ablated TiO_2 target (third line), and at 122 nm below the surface of an ablated TiO_2 target (upper line). The Ti 2p spectrum for the fresh target surface shows two peaks at 458.3 eV and 463.9 eV (2$p_{3/2}$ and 2$p_{1/2}$, respectively), and the corresponding peak in the O 1s spectrum is positioned at 529.3 eV, all indicative of stoichiometric TiO_2 [20]. The peaks shift to 458.1 eV, 463.5 eV, and 529.9 eV, respectively, due to oxygen loss during argon etching. The Ti 2p spectrum for the ablated target at 122 nm below the target surface shows two large peaks at 460.0 eV and 455.0 eV, and a small side lob at 454.0 eV belonging to a metallic form of Ti. The O 1s spectrum has a peak at 530.6 eV. The target material is, indeed, strongly reduced during ablation, resulting in Ti-rich material.

5   Discussion

Periodic surface structures induced by repetitive laser irradiation on stationary targets have been observed for a wide class of target materials such as metals [21], ceramics [22], polymers [23], and semiconductors [24, 25]. Sipe et al. [26] considered that the periodic structures result from inhomogeneous energy profiles associated with the interference of the incident beam with a surface-scattered field for fluences near the damage threshold (< 0.55 J cm^{-2}). The pattern spacings for polarized light were determined to be $\lambda(1 \pm \sin\theta)^{-1}$ and $\lambda(\cos\theta)^{-1}$, where λ is the wavelength of the laser beam and θ the angle of incidence of the beam. In this study, unpolarized light of higher fluence was used, which induced larger spacings as also reported by others [24, 27]. Clark and Emmony [28] discussed the possibility of interfer-

ing or beating waves resulting in larger spacings. They also attributed wave-like structures to frozen capillary waves. Capillary waves can be generated as a result of the impulse that the target surface suffers when material is ablated from it. This impulse would seed capillary waves in the same way that dropping a stone into a lake generates waves. The ripple spacing is then determined primarily by how long the impulse lasts, which in turn depends largely on the time the surface stays molten. The target material must freeze before the waves decay away to create the periodic target structure. Since short-wavelength structures have the fastest decay, they are more likely to decay away before the target surface is solid again. Finally, the wavelength of the light incident on the target surface can be much larger than the free-space wavelength, because of the presence of a plasma close to the target surface. If the refractive index of the plasma were smaller than 1, the wavelength of the laser pulse as seen by the surface would be increased due to passage through the plasma.

The desirable smooth surface after ablation was only achieved in the case of $SrTiO_3$ and $BaTiO_3$ ablation. It was not possible to induce the same smooth morphology in the case of TiO_2 ablation. Apparently, TiO_2 ablation characteristics fall in between those of the ablated metals and perovskites, not achieving a flat surface but showing some periodic surface structure, although not as strong as in the case of metal ablation. The metal and oxide properties differ mostly for the reflectance, thermal conductivity, and enthalpy of evaporation. Looking at the values of the physical parameters given in Table 1, TiO_2 characterization falls in between the values for metals and oxides in the case of the enthalpy of evaporation, H_{ev}. Its estimated H_{ev} is a factor of two to five higher than those of the metals but a factor of two lower than those of the other oxides. The enthalpy of evaporation can be regarded as a cooling source at the target surface. A higher H_{ev} in combination with a lower κ for $SrTiO_3$ and $BaTiO_3$ confines the absorbed energy to the target surface. The lower H_{ev} in combination with the higher κ for the metals makes the energy absorption more a target volume process in comparison with $SrTiO_3$ and $BaTiO_3$.

Span [29] investigated the dependence of surface target morphology and relative composition of a $La_{0.5}Sr_{0.5}CoO_3$ target after ablation as a function of fluence. For low fluences

$(0.3–0.4\,\mathrm{J\,cm^{-2}})$, large cones were formed at the target surface directed along the laser beam. The top of the cones consisted of refractory Co nuclei with a higher ablation threshold, shielding the stoichiometric target material from ablation. Dam et al. [2] studied the phase separation induced by incongruent melting in a $YBa_2Cu_3O_{7-\delta}$ target, leaving a Y-enriched surface behind at low fluences. The Ti enrichment observed in this study induces changes in the optical and thermal properties of the TiO_2 target during ablation. However, TiO, TiO_2, Ti_2O_3, Ti_3O_5, and pure Ti all have about the same melting point. The reflectance of Ti is similar to the reflectance of TiO_2 at 248 nm, and its specific heat is similar to those of Ni and Fe. The main differences are found for the absorption coefficient and, therefore, penetration depth, and the thermal conductivity. Ti does have twice as a large thermal conductivity as TiO_2, which is still four times lower than for Ni and Fe. The penetration depth of Ti is 23.5 nm for 248-nm irradiation, which is three times larger than for the other materials used in this study. The larger thermal conductivity and penetration depth result in a higher ablation threshold for Ti in comparison with TiO_2. If the top layer of the ridges present in the TiO_2 target morphology after ablation at $1.5\,\mathrm{J\,cm^{-2}}$ (see Fig. 5b) consists of Ti, it can shield the underlying stoichiometric target material from ablation. So, the observed TiO_2 target ablation characteristics fall in between those of the ablated metals and perovskites, because ablation results in the presence of Ti-rich material, whose values for the thermal diffusivity falls in between the values for the other metal and oxides used in this research, while its penetration depth is larger.

6 Conclusion

The influence of the laser fluence and the number of laser pulses on the resulting morphology of metal (Ni, Fe, Nb) and oxide (TiO_2, $SrTiO_3$, $BaTiO_3$) targets have been presented. Although different responses for metal and oxide targets to repetitive laser irradiation could be expected due to the different band structures of metals and oxides, the optical response is quite similar for 248-nm laser irradiation. Therefore, the difference in response is largely caused by differences in thermal properties such as thermal conductivity and enthalpy of evaporation. A flat target morphology after target ablation is desirable for a stable use of the target during thin-film deposition. However, this is not achievable for all materials. Metal targets show periodic structures of the order of micrometers after consecutive pulses of laser radiation, but the $SrTiO_3$ and $BaTiO_3$ targets show a flat surface after ablation for relatively low fluences $(1.0\,\mathrm{J\,cm^{-2}})$. The observed TiO_2 target ablation characteristics fall in between those of the ablated metals and perovskites, because ablation results in Ti-rich material, whose values for the thermal conductivity, specific heat, and the absorption coefficient are different from those of TiO_2. The straight ridges present in the TiO_2 target morphology after ablation at $1.5\,\mathrm{J\,cm^{-2}}$ ap-

pear to be caused by the presence of Ti in their top layers, shielding the underlying stoichiometric target material from ablation. The final target morphology is dependent on fluence, number of pulses, and the movement of the target itself (rotating, scanning, or stationary). It can take between 15 and 75 pulses to reach a steady-state target morphology on a stationary target.

REFERENCES

1 E.A.F. Span, F.J.G. Roesthuis, D.H.A. Blank, H. Rogalla: Appl. Surf. Sci. **150**, 171 (1999)
2 B. Dam, J.H. Rector, J. Johansson, S. Kars, R. Griessen: Appl. Surf. Sci. **96–98**, 679 (1996)
3 I.W. Boyd: *Laser Processing of Thin Films and Microstructures* (Springer, Berlin 1987)
4 P.R. Willmott, J.R. Huber: Rev. Mod. Phys. **72**, 315 (2000)
5 E.D. Palik: *Handbook of Optical Constants of Solids* (Academic, Orlando, FL 1985)
6 E.D. Palik: *Handbook of Optical Constants of Solids II* (Academic, San Diego, CA 1991)
7 M. von Allmen, A. Blatter: *Laser-beam Interactions with Materials: Physical Principles and Applications* (Springer, Berlin 1995)
8 R. Wood: *Laser Damage in Optical Materials* (IOP, Bristol 1990)
9 http://www.webelements.com/
10 G. Grimvall: *Thermophysical Properties of Materials* (Elsevier, Amsterdam 1999)
11 M.K. Karapet'yants, M.L. Karapet'yants: *Thermodynamic Constants of Inorganic and Organic Compounds* (Ann Arbor–Humphrey Science, London 1970)
12 D.R. Lide: *CRC Handbook of Chemistry and Physics, Vol. 81* (CRC, Boca Raton, FL 2000)
13 F. Cardarelli: *Materials Handbook* (Springer, London 2000)
14 Y. Hiroshima, T. Ishiguro, I. Urata, H. Makita, H. Ohta, M. Tohogi, Y. Ichinose: J. Appl. Phys. **79**, 3572 (1996)
15 E. Matthias, M. Reichling, J. Siegel, O.W. Käding, S. Petzoldt, H. Skurk, P. Bizenberger, E. Neske: Appl. Phys. A **58**, 129 (1994)
16 B. Knacke: *Thermochemical Properties of Inorganic Substances* (Springer, Berlin 1973)
17 S. Fähler, H.-U. Krebs: Appl. Surf. Sci. **96–98**, 61 (1996)
18 R. Jordan, J.G. Lunney: Appl. Surf. Sci. **127–129**, 968 (1998)
19 H.-A. Durand, J.-H. Brimaud, O. Hellman, H. Shibata, S. Sakuragi, Y. Makita, D. Gesbert, P. Meyrueis: Appl. Surf. Sci. **86**, 122 (1995)
20 J.F. Moulder, W.F. Stickle, P.E. Sobol, K.E. Bomben: *Handbook of X-ray Photoelectron Spectroscopy* (Perkin-Elmer, Eden Prairie, MN 1992)
21 J.F. Young, J.S. Preston, H.M. van Driel, J.E. Sipe: Phys. Rev. B **27**, 1155 (1983)
22 L.M. Doeswijk, H.H.C. de Moor, D.H.A. Blank, H. Rogalla: Appl. Phys. A **69**, S409 (1999)
23 P. Milani, M. Manfredini: Appl. Phys. Lett. **68**, 1769 (1996)
24 D.H. Lowndes, J.D. Fowlkes, A.J. Pedraza: Appl. Surf. Sci. **154–155**, 647 (2000)
25 J.F. Young, J.E. Sipe, H.M. Driel: Phys. Rev. B **30**, 2001 (1984)
26 J.E. Sipe, J.F. Young, J.S. Preston, H.M. van Driel: Phys. Rev. B **27**, 1141 (1983)
27 E. György, I.N. Mihailescu, P. Serra, A. Pérez del Pino, J.L. Morenza: Surf. Coat. Technol. **154**, 63 (2002)
28 S.E. Clark, D.C. Emmony: Phys. Rev. B **40**, 2031 (1989)
29 E.A.F. Span: *Oxygen-permeable Perovskite Thin-film Membranes by Pulsed Laser Deposition*. Ph.D. thesis, University of Twente, The Netherlands (2001)